Hindawi
Advances in Polymer Technology
Volume 2019, Article ID 4682164, 13 pages
https://doi.org/10.1155/2019/4682164

Research Article

Preparation of LDHs Based on Bittern and Its Flame Retardant Properties in EVA/LDHs Composites

Long Li, Yi Qian, Peng Qiao, Haoyue Han, and Haiming Zhang

College of Environment and Safety Engineering, Qingdao University of Science and Technology, Qingdao 266042, China

Correspondence should be addressed to Yi Qian; qianyi1962@126.com

Received 15 October 2018; Revised 25 January 2019; Accepted 17 February 2019; Published 1 April 2019

Academic Editor: Camino Giovanni

Bittern, as a byproduct of salt manufacture, is abundant in China. The researches and developments for seawater bittern have mainly focused on the reuse of magnesium, calcium, lithium, and boron. However, the utilization rate is less than 20%. The large amount of unused bittern has become a challenge that attracts much attention in academic and industry areas. In this paper, three kinds of layered double hydroxides (LDHs) were synthesized from bittern using a coprecipitation method and characterized by X-ray diffraction (XRD). The XRD results showed that the three kinds of LDHs(MgAl-LDHs, MgFe-LDHs and MgAlFe-LDHs) were successfully synthesized. Then, the flame retardant properties and thermal properties of the three LDHs in ethylene vinyl acetate (EVA)/LDHs composites had been tested by cone calorimeter test (CCT), limiting oxygen index (LOI), smoke density test (SDT), and thermogravimetry-Fourier transform infrared spectrometry (TG-IR). The CCT results showed that the heat release rate (HRR) of all three kinds of EVA/LDHs composites significantly decreased compared with that of pure EVA, and the EVA/MgAl-LDHs composites had the lowest PHRR value of 222.65 kW/m^2. The LOI results showed that EVA/MgAl-LDHs composites had the highest LOI value of 29.8%. The SDT results indicated that MgAl-LDHs were beneficial to smoke suppression. TG-IR results showed that EVA/MgAl-LDHs composites had a better thermal stability.

1. Introduction

Seawater bittern, or called brine, is a byproduct of salt manufacture, which is generally regarded as a typical solid waste [1]. As the world's largest producer of sea salt, about 2×10^7 cubic meters of bittern was produced every year in China. Though the bittern resources are very rich in China, the utilization rate is low, even less than 20%. Large amount of waste bittern has become a challenge that attracts much attention in water industry [2–4]. The byproduct is rich in magnesium, potassium, bromine, etc. Its Mg^{2+} content is about 32 g/L, as 27 times as that of seawater [5], so bittern is considered to be one of the ideal resources to extract magnesium salt.

At present, the methods to reuse bittern mainly focused on the purifications of magnesium, potassium, bromine, and lithium products [6, 7]. Besides, bittern has also been used as efficient chemicals to treat sewage [8–10]. Moreover, bittern can also be used as coagulant along with lime, and the results showed that the amount of lime/bittern coagulation had great effects on the characteristics and quantities of sludge and then in turn influence the sewage disposal results. Bittern also has some interesting agricultural uses [11–13]. For example, P.A. Davies [1] used bittern as a source of liquid desiccant for cooling to greenhouses, which makes crop a good production in hot climates. Furthermore, Xu Hui [14] prepared superfine magnesium hydroxide flame retardant using bittern and ammonia, and the properties of the products are so good that can be applied as flame retardant additives of polymers. In this paper, bittern is used to prepare layered double hydroxides (LDHs), which is another environmental friendly flame retardant.

LDHs are called anionic layered clays, and its general formula can be described by $[M_{1-x}^{2+}M_x^{3+}(OH)_2]A_{x/n}^{n-}\cdot mH_2O$. M^{2+} is for divalent metal ions, M^{3+} for trivalent metal ions, and A^{n-} for interlayer anion [15]. Typical LDH is $Mg_6Al_2(OH)_{16}CO_3\cdot4H_2O$ and its structure is similar to $Mg(OH)_2$[16]. Because of their special structure, it have been widely used as flame retardant, catalyst [17, 18], medicine [19, 20], for treating of wastewater [21], and so on. As a

flame retardant, it has advantages such as nonhalogenated, nontoxic, and no corrosive gas generation when added into polymer matrices [16]. In recent years, LDHs and many other kinds of green derived materials have been used as efficient flame retardant materials [22–25].

In this paper, three kinds of LDHs (MgAl-LDHs, MgFe-LDHs, and MgAlFe-LDHs) were synthesized based on bittern by a coprecipitation method and characterized by XRD and TGA. Then, they were used into EVA as a flame retardant. And the flame retardant properties and thermal properties of these EVA/LDHs composites have been tested by LOI, CCT, SDT, and TG-IR. Actually, this is the first time that LDHs have been synthesized from bittern and then used as efficient flame retardant materials for EVA. We believe that this work will broad the way for the reuse and recovery of solid waste.

2. Experimental

2.1. Materials. Bittern was supplied by Weidong Chemical Saltwork. It contains Mg (31882.64μg/g), K(4284.47μg/g), Na(31854.06μg/g), Fe(12.04μg/g), Al(5.08μg/g), Cr(6.58μg/g), and Zn(1.99μg/g). The result is examined by inductively coupled plasma atomic emission spectrometry (ICP-AES). EVA with vinyl acetate of 18% was bought from Beijing Eastern Petrochemical (China).

2.2. Syntheses of LDHs

Synthesis of MgAl-LDHs. Bittern was prepared after filtration. Then, $AlCl_3{\cdot}6H_2O$ and bittern were mixed with M^{2+}/M^{3+} molar ratios of 3.0/1.0(Solution A). The solution of strong base which contained 0.4mol·L^{-1} Na_2CO_3, 1.5mol·L^{-1} NaOH was prepared (Solution B). Then, solutions A and B were added at the same speed to a three-necked flask with the condition of water-bath heating and constant speed stirring. The stirring speed kept unchanged and the temperature was 80°C. After the reaction finished, the reaction product was washed to pH=7 and dried at 80°C to obtain MgAl-LDHs.

Synthesis of MgFe-LDHs. Repeat the steps *Synthesis of MgAl-LDHs* by replacing $AlCl_3{\cdot}6H_2O$ with $FeCl_3{\cdot}6H_2O$ to produce MgAl-LDHs.

Synthesis of MgAlFe-LDHs. Repeat the steps *Synthesis of MgAl-LDHs* by replacing $AlCl_3{\cdot}6H_2O$ with $AlCl_3{\cdot}6H_2O$ and $FeCl_3{\cdot}6H_2O$ (the molar ratios is 1:1) to produce MgAlFe–LDHs.

2.3. Preparation of EVA/LDHs Composites. The LDHs samples and EVA were added into a mixer together and were melt-compounded at 120°C for 10 min. Then, the mixtures were compression-molded at 120°C into sheets under a pressure of 10 MPa for 10 min. Last, the sheets were cut into different sized specimens for flame retardant tests. In this work, the additive level of all samples was 50%, and the samples were named EVA0 (pure EVA), EVA1 (containing 50% MgAl-LDHs), EVA2 (containing 50% MgFe-LDHs), and EVA3 (containing 50% MgAlFe-LDHs).

2.4. Experimental Equipment

2.4.1. X-Ray Diffraction (XRD). XRD results were recorded on a Philips *X*'Pert Pro Super apparatus (Nicolet Instrument Co., Madison, WI) using Cu Ka radiation with a nickel filter (wavelength =1.5418Å) at a scan rate of 0.0167°/s.

2.4.2. Thermogravimetric Analysis (TGA). TGA of the cured sample was performed using a DT-50 (Setaram, France) instrument. About 10.0 mg of sample was put in an alumina crucible and heated from 25 to 700°C. The heating rate was set as 10 K/min (nitrogen atmosphere, flow rate of 20 ml/min).

2.4.3. Scanning Electron Microscopy (SEM). The SEM studies were performed using a Hitachi X650 scanning electron microscope at an accelerating voltage of 8 kV.

2.4.4. Cone Calorimeter Test (CCT). The CCT (Stanton Redcroft, UK) were performed according to ISO 5660 standard procedures. Each specimen was in size of 100×100×4 mm^3, and it was wrapped in aluminum foil and exposed horizontally to an external heat flux of 50 kW/m^2.

2.4.5. Limiting Oxygen Index (LOI). LOI was measured according to ASTM D 2863. The apparatus used was an HC-2 oxygen index meter (Jiangning Analysis Instrument Company, China). The specimens used for the test were of dimensions 100×6.5×3 mm^3.

2.5. Smoke Density Test(SDT). A Smoke density test machine JQMY-2 (Jianqiao Co, China) was used to measure the smoke characteristics according to ISO 5659-2(2006). Each specimen of dimensions 75×75×2.5 mm^3 was wrapped in aluminum foil and exposed horizontally to an external heat flux of 25 kW/m^2 with or without the application of a pilot flame.

2.6. Thermogravimetry-Fourier Transform Infrared Spectrometry (TG-IR). The TG-IR instrument consist of a thermogravimeter (TG2009 F1, Netzsch Instruments, Germany), a Fourier transform infrared spectrometer (Vertex 70, Bruker Optics, Germany), and a transfer tube with an inner diameter of 1 mm connected to the TG and the infrared cell. The investigation was carried out from 30 to 800°C at a linear heating rate of 10°C/min under the nitrogen flow rate of 3×10^{-5} m^3/min.

3. Results and Discussion

3.1. XRD of LDHs. XRD patterns of three kinds of LDHs are shown in Figure 1. All the LDHs samples showed peaks at 12, 24, 35, 39, 61, and 62, which correspond to the characteristic peak of (003), (006), (009), (015), (110), and (113). The diffraction peak of (003) is a typical characteristic peak of the hydrotalcite-type materials and the high intensity indicating the good crystallinity degree. Moreover, the crystal planes of peaks (110) and (113) are clearly separated, indicating a

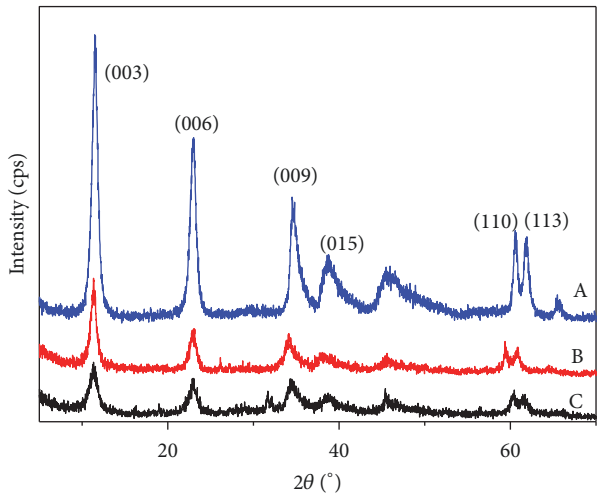

Figure 1: XRD patterns of LDHs samples (A: MgAl-LDHs, B: MgFe-LDHs, and C: MgAlFe-LDHs).

high degree of regularity among anion layers [26]. The unit cell parameter *a* represents the average distance between two metal ions in the layers and *c* represents the layer spacing of the materials. The value *a* of three samples is all 0.31nm and the value *c* is 2.31nm, 2.34nm, and 2.35nm, which are close to the value previously reported [27, 28]. And it proves that LDHs can be synthesized successfully using bittern with M^{2+}/M^{3+} molar ratios of 3.0/1.0.

In addition, XRD pattern of MgAl-LDHs shows more sharper and symmetrical peaks than that of the other two, which indicating the well-formed crystalline layered structures of MgAl-LDHs [29, 30]. The *c* value of MgAl-LDHs is 2.31nm, lower than MgFe-LDHs and MgAlFe-LDHs, which means that the layer space is enlarged. The reason may be that the addition of Fe^{3+} weakened the electrostatic attraction between the layer board and the layers.

3.2. SEM of LDHs. The morphologies of LDHs powder are shown in Figure 2. Agglomerates can be found in all the three kinds of LDHs samples. The average size is 500 nm, 400 nm, and 600 nm for MgAl-LDHs, MgFe-LDHs, and MgAlFe-LDHs, respectively. It is clear that the particles of MgAlFe-LDHs are bigger than the other two LDHs. Roughly, it can be concluded that the distribution of the particle size is small, which may contribute a better compatibility with polymer matrix.

3.3. TGA Characterization of LDHs. Thermogravimetric (TG) and derivative thermogravimetric (DTG) curves of the LDHs are shown in Figures 3 and 4, and related data can be found in Table 1. It can be seen that thermal decomposition of LDHs contains two processes. The first decomposition step occurs from 100 to 300°C, with the mass loss of 17 wt%(MgAl-LDHs), 13 wt% (MgFe-LDHs), and 14 wt%(MgAlFe-LDHs), respectively. During this process, LDHs lose adsorbed water on the surface and the crystallization water in the interlayer space [29, 31]. The second step occurs after 300°C with

Table 1: Decomposition steps and mass loss from TG.

Sample code	First Step (°C)	Mass Loss (%)	Second Step (°C)	Mass Loss (%)
MgAl-LDHs	203±4	17±1	380±2	32±0.6
MgFe-LDHs	210±3	13±0.5	375±3	23±0.7
MgAlFe-LDHs	199±3	14±0.6	379±2	32±0.5

mass loss of 32 wt%(MgAl-LDHs), 23 wt%(MgFe-LDHs), and 32 wt% (MgAlFe-LDHs). During this period, LDHs lose the OH^- and CO_3^{2-} ions between interlayers and then the structures of LDHs were completely destroyed [29, 31].

Figures 3 and 4 also show that the second decomposition temperature of MgFe-LDHs is lower than that of the other two, indicating that the addition of Fe will reduce the thermostability of LDHs. It can also be seen that MgAl-LDHs lose more weight with a residue of 51 wt%, while 54 wt% and 64 wt% residue were observed for MgAlFe-LDHs and MgFe-LDHs. The reason may be that MgAl-LDHs with good crystallinity structure can accommodate more water and anions.

3.4. Flammability Behavior of EVA/LDHs Composites

3.4.1. CCT Results of EVA/LDHs Composites. CCT is widely used for assessing the fire reaction behavior of polymer materials which can provide many information to describe the combustion process, such as heat release rate (HRR), mass, total heat release (THR), mass loss rate (MLR), time to ignition (TTI), and smoke production rate (SPR) [32–34].

HRR of EVA/LDHs Composites. HRR plots of EVA/LDHs composites are shown in Figure 5(a) and more important numerical data are listed in Table 2. HRR refers to the heat release rate per unit area, which is one of the most important parameters of fire behaviors [35]. As is shown, the HRR curve of EVA0 (pure EVA) rises up quickly after ignition. It reaches the peak of heat release rate (PHRR) of 1645.88 kW/m^2 in only 200s and exhibits a TTI of 38s. When 50 wt% LDHs were introduced into pure EVA, the values of PHRR and TTI decreased significantly in comparison with virginal EVA. Firstly, the PHRR of EVA1 ~ EVA3 were all below 320 kW/m^2. Secondly, the TTI was prolonged to 44~72s. As a result, significant improvement in the fire retardant properties was observed by addition of LDHs into EVA.

From Figure 5(a) and Table 2, we can also see that EVA1(with MgAl-LDHs) has a better fire retardant performance. EVA1 shows a lowest PHRR value of 222.65 kW/m^2, while the value of EVA2 (with MgFe-LDHs) and EVA3 (with MgAlFe-LDHs) is 311.87 kW/m^2 and 286.96 kW/m^2, respectively. Moreover, the ignition time of EVA1 is 72s, while the value for EVA2 and EVA3 is 44s and 48s. This phenomenon fits well with the XRD and TGA results, indicating that a good crystallinity structure may be beneficial to improve the fire retardant properties.

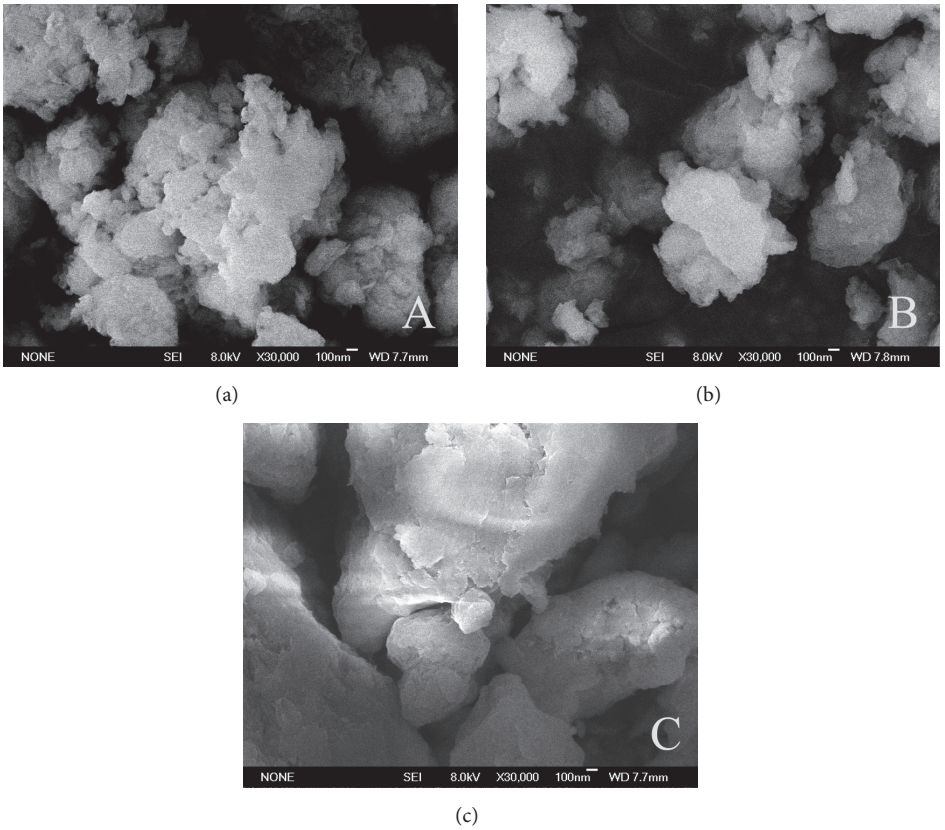

(a) (b) (c)

Figure 2: SEM of LDHs samples ((a) MgAl-LDHs, (b) MgFe-LDHs, and (c) MgAlFe-LDHs).

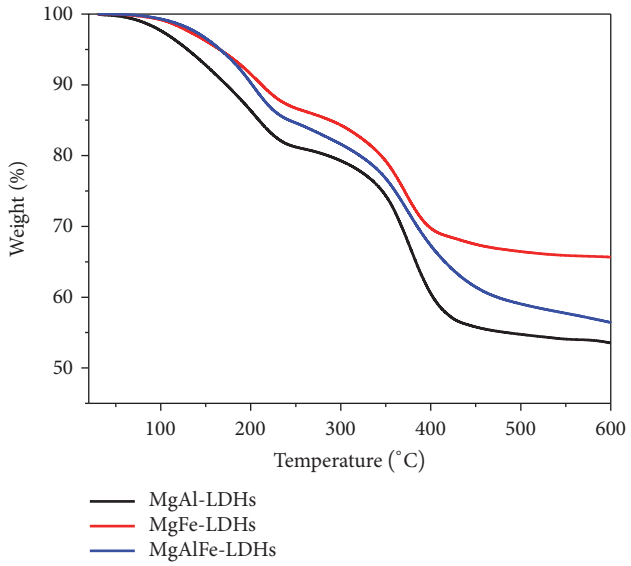

Figure 3: TG curves of LDHs.

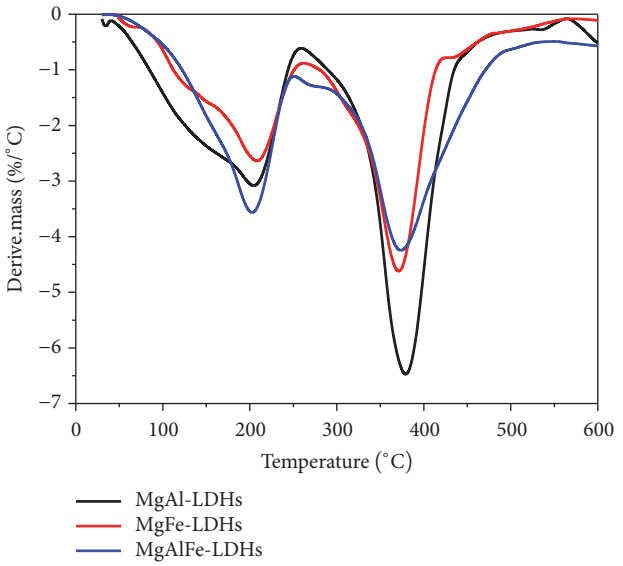

Figure 4: DTG curves of three kinds of LDHs.

THR of EVA/LDHs Composites. Figure 5(b) presents the THR curves of four samples. The curve of EVA0 rises up quickly, which is in accordance with the HRR curve. And it exhibits a THR of 145.41 MJ/m^2, which is larger than the values for EVA1 (121.48 MJ/m^2), EVA2 (123.99 MJ/m^2), and EVA3 (111.97 MJ/m^2). It is clear that LDHs is helpful for reducing the THR of EVA/LDHs composites.

MASS of EVA/LDHs Composites. The MASS of the char residues is shown in Figure 5(c). The curves show the same

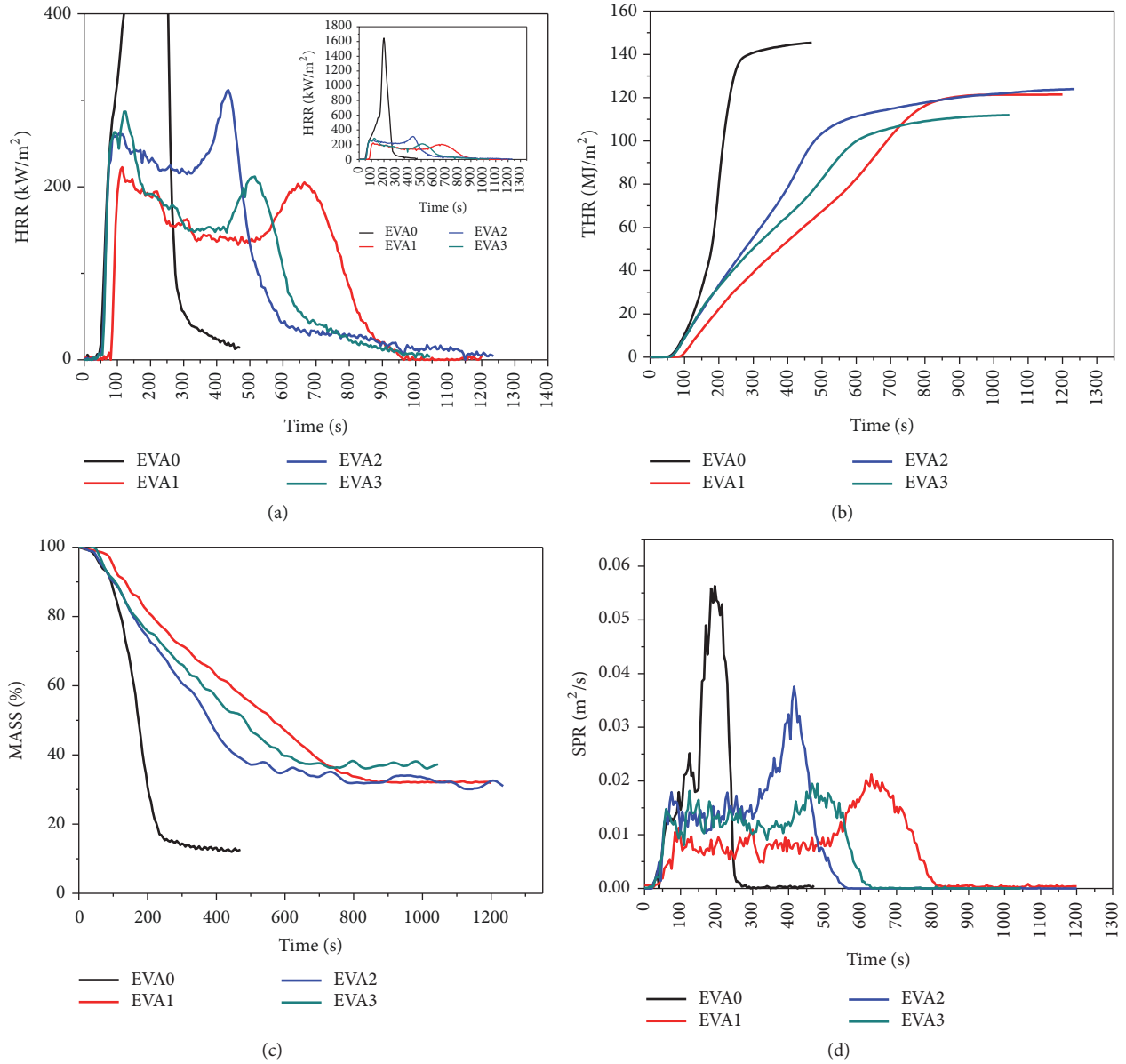

Figure 5: Cone curves of EVA/LDHs composites ((a) HRR, (b) THR, (c) mass, and (d) SPR).

trend with HRR for EVA0~EVA3. EVA0 completes the burning process quicker compared with EVA1~EVA3. Pure EVA left almost nothing after combustion, while the residue rate for EVA1~EVA3 is 32%, 31%, and 37%, respectively. For EVA1~EVA3, a charred layer may be formed at the beginning of the combustion, which can slow down the combustion process. Besides that, LDHs can release CO_2 under high temperature, which can cover the flame and dilute flammable gas. With the development of combustion process, the charred layer begins to break, resulting in large mass loss of the composites.

SPR of EVA/LDHs Composites. SPR is used to evaluate the rate of smoke generation. As shown in Figure 5(d), the SPR curve of EVA0 rises up rapidly, and it reaches the peak of SPR (PSPR) in only 195s. In comparison with pure EVA, the curves of EVA1~EVA3 are more flat and the PSPR values decrease. Moreover, the time to PSPR is prolonged to 630s, 420s, and 475s for EVA1~EVA3. The phenomenon fit well with the curves of HRR, indicating that smoke emission of EVA is retarded by added LDHs.

Digital Photos of Residues. Figure 6 exhibits the residues of EVA/LDHs composites after CCT. It is clear to see that EVA0 sample leaves no charred residues at the end of combustion. From Figure 7, it can be seen that the charred residues of EVA2 and EVA3 are compact and integrated, while the charred residue of EVA1 is loose and incomplete. The possible reason is that the addition of Fe element is helpful to form a better charred layer. Moreover, CO_2 and metallic oxide may

Table 2: Data from CCT.

Sample code	PHRR (kW/m^2)	Time to PHRR(s)	THR (MJ/m^2)	TTI (s)	Time to flame out (s)
EVA0	1645.88±8	200±5	145.41±0.3	38±4	352±5
EVA1	222.65±10	115±3	121.48±0.4	72±3	875±6
EVA2	311.87±9	435±4	123.99±0.3	44±3	598±4
EVA3	286.96±9	120±4	111.97±0.3	48±3	710±5

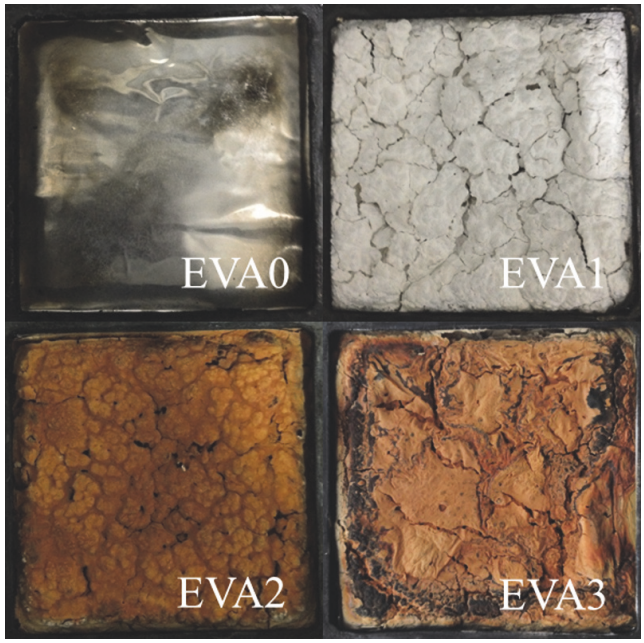

Figure 6: Photographs after cone calorimeter test.

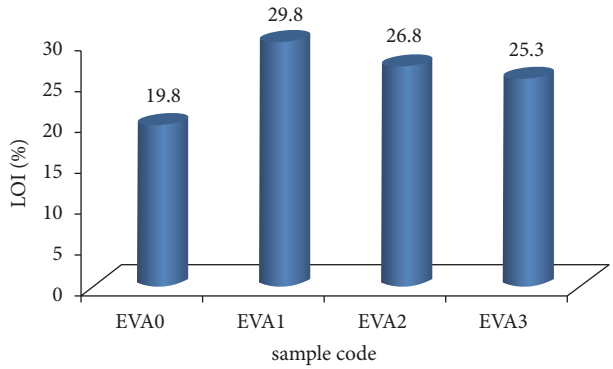

Figure 7: LOI values of EVA/LDHs composites.

be produced from destroyed LDHs under high temperature, which can lower the temperature and dilute combustible gas.

3.4.2. LOI Results of EVA/LDHs Composites. Limiting oxygen index (LOI) is a qualitative method to evaluate the flame retardancy of polymeric materials [36]. Figure 7 presents the LOI values of all samples and the value of pure EVA is only 19.8%, which increases by addition of LDHs. The LOI value for EVA1 reaches up to 29.8%, the most one among three samples. These results are consistent with the results mentioned above.

3.4.3. SDT of EVA/LDHs Composites. SDT is usually used to evaluate the smoke suppression character, which gives detailed information about the smoke production [33]. As is shown in Figure 8, the EVA0 sample produces a great amount of smoke and its luminous flux gets to 0% in a short time. In Figure 8(a), when a flame source is used, EVA1 produces less smoke than EVA2 and EVA3 before 1100s. After 1100s, EVA1 produces more smoke than EVA2, which may be owing to the fact that the char layer formed by EVA1 is not compact and is broken under high temperature. In Figure 8(b), the smoke production of EVA2 is the largest. These results fit well with the CCT results, indicating that LDHs can suppress the smoke production. Good performances of the composites in SDT test are due to the decomposition of LDHs and the following formed char layer, which have been mentioned previously. It should also be noticed that when a flame source is used, the sample produces less smoke, which can be ascribed to the materials' incomplete combustion. The solid particles produced by incomplete combustion will immediately transfer to the gas phase, increasing the amount of smoke [34].

3.4.4. TG-IR of EVA/LDHs Composites

TG Behavior of the EVA/LDHs Composites. Figures 9 and 10 present the TG and DTG curves of pure EVA and its composites. It is observed that the pyrolytic decomposition of EVA0 is a two-step process. It is clear to see that Step 1 occurs in the range of 290~390°C with T_{max} of 356°C; the main process in this step is decarboxylation of EVA, generating H_2O and CO_2. Step 2 takes place in the range of 390~500°C with T_{max} of 471°C, only 0.05% residue left at the end of this process. During this step, the main chain of EVA begins to rupture, producing olefins like butene and ethylene [36].

Different from pure EVA, pyrolytic decomposition of the EVA/LDHs composites can be accomplished in three steps. In general, EVA1 shows better thermal stability than the other two samples. For EVA1, the first step occurs in the range of 100~250°C with T_{max} of 215°C; LDHs lost the water bounded in the interlayer space in this step. The second step occurs in the range of 250~390°C with T_{max} of 357°C, which corresponds to the dehydroxylation and decarbonization of LDHs. And the third step occurs after 390°C with T_{max} of 472°C, which is attributed to the decarboxylation and main chain rupture of EVA. For EVA2, T_{max} of three steps are 134, 364, and 472°C. For EVA3, T_{max} of three steps are 173, 363, and 472°C. It is obvious to see that the temperature of pyrolytic decomposition is lower than that of EVA1. Moreover, EVA1 ends up pyrolytic decomposition with a residue of 28.6 wt%, while the values for EVA2 and EVA3 are 36.5 wt% and 26.6 wt%, respectively. This phenomenon fits well with the TGA results of LDHs. That is to say, MgAl-LDHs can accommodate more water and anions, resulting in the largest mass loss among three samples.

FTIR Characterization of the EVA/LDHs Composites. 3D TG-FTIR spectra of pyrolysis products of the pure EVA and EVA/LDHs composites during the thermal degradation are depicted in Figure 11. The figures show that the gas products of the four samples exhibit characteristic bands at 3400–4000 cm^{-1}, 2800–3150 cm^{-1}, 2250–2400 cm^{-1}, 1700–1850 cm^{-1}, 1250–1500 cm^{-1}, and 950–1150 cm^{-1}, which correspond to H_2O (3400–4000 cm^{-1}), CO_2 (2300–2400 cm^{-1}), CO (2250–2300 cm^{-1}), carboxylic acid (1700–1850 cm^{-1}), and

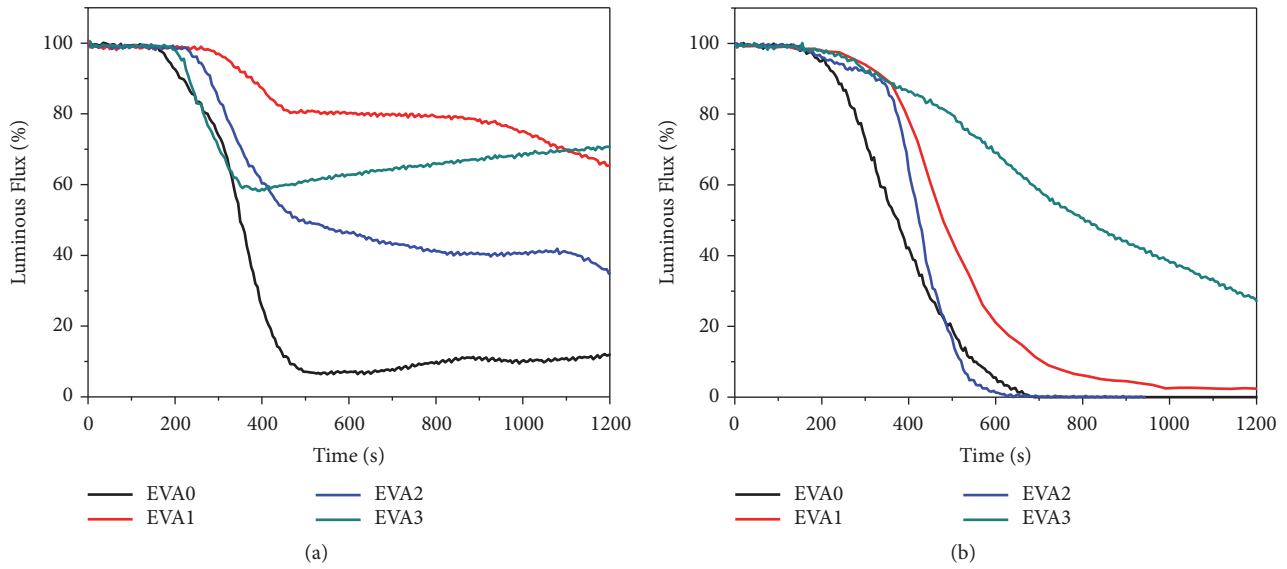

Figure 8: Luminous flux curves of EVA/LDHs composites: (a) with the application of a pilot flame and (b) without the application of a pilot flame.

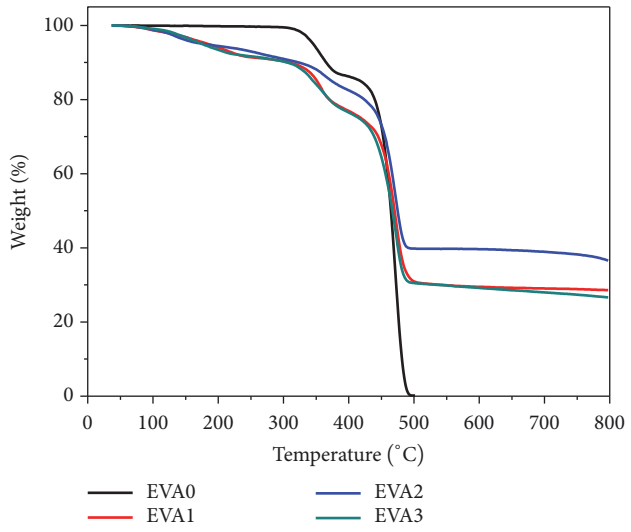

Figure 9: TG curves of EVA/LDHs composites.

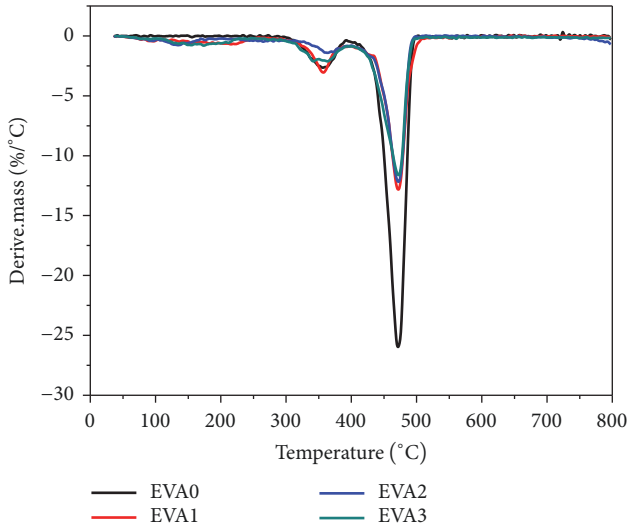

Figure 10: DTG curves of the EVA/LDHs composites.

aliphatic hydrocarbon (2800–3150 cm^{-1}, 1250–1500 cm^{-1}, and 950–1150 cm^{-1}), respectively [33, 37, 38]. It is clear that pure EVA produces more carboxylic acid and aliphatic hydrocarbon, while EVA/LDHs composites produce more CO_2 during the thermal degradation. This phenomenon fits well the TG results.

The characteristic FTIR spectrum of pyrolysis products of EVA0~EVA3 in the temperature range of 30~900°C during the thermal degradation is shown in Figure 12. As shown, there is almost no infrared signal for pure EVA below 300°C. However, a peak attributed to CO_2 can be seen at about 295°C for EVA1 and EVA2 and about 225°C for EVA3. It means that the EVA1~EVA3 begin to decompose at this temperature, while pure EVA do not decompose under this situation. The intercated CO_3^{2-} in LDHs is the main reason for the released CO_2 from EVA/LDHs composites.

With the raise of the temperature, the signals of CO, CO_2, and H_2O could be detected. The fact is that pure EVA produce more carboxylic acid than EVA1~EVA3. The reason may be that LDHs can transfer carboxylic acid into CO_2 and H_2O. As is shown in Figures 11 and 12, a sharp peak at about 460°C appears for all the samples, which means aliphatic hydrocarbons generated. The detected signals of aliphatic hydrocarbons certificate the ruptures of main chain. When LDHs are added into EVA, the release of aliphatic hydrocarbons is decreased significantly and the temperature at which main chain break gets lower slightly.

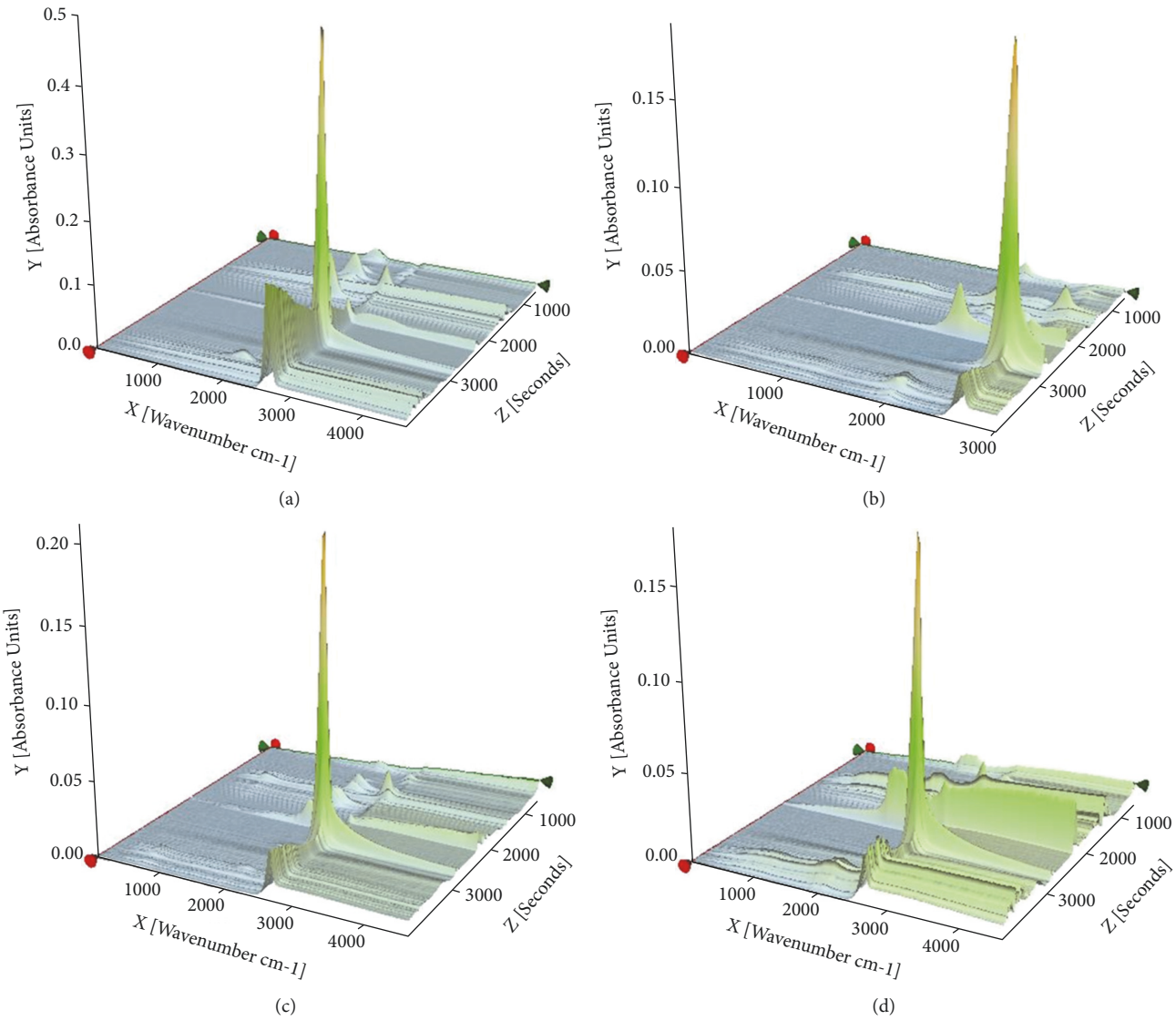

Figure 11: 3D TG-FTIR spectra of pyrolysis products of the composites during the thermal degradation: (a) EVA0, (b) EVA1, (c) EVA2, and (d) EVA3.

Figure 13 shows some detailed data about the pyrolysis products of EVA0~EVA3 at different temperatures. From Figure 13(a), it is clear that the H_2O release of EVA0 is a two-step process. Pure EVA begins to release water at about 330°C and reaches its first peak at about 370°C. And the second step starts from 400°C, the release of H_2O keeps growing along with the temperature. For EVA1~EVA3, the process of H_2O release has three steps, and EVA1 releases more H_2O than other samples, which is in accordance with the DTG results above. From Figures 13(b) and 13(c), it can be found that almost no peaks for EVA0 are observed until about 500°C, indicating that there is no released CO_2, while peaks are found at about 350°C for EVA/LDHs samples. Moreover, the release of CO is reduced significantly when LDHs is added to EVA. It is believed that the combustion products of LDHs can promote carbon formation, resulting in the reduction of CO. It can be seen in Figures 13(d) and 13(e) that EVA0 shows a sharp peak at about 470°C and it produces more carboxylic acid and aliphatic hydrocarbons than EVA/LDHs samples. It is reasonable considering that LDHs can react with carboxylic acid and aliphatic hydrocarbons to form H_2O; thus the release of carboxylic acid and aliphatic hydrocarbons is maintained at a low level. From these results, it can be concluded that MgAl-LDHs is an efficient flame retardant to EVA.

Many papers have been published describing the flame retardant properties of EVA-LDH composites. A range of various LDHs including MgAl-CO_3, ZnMgAl-CO_3, MgAlFe-CO_3, MgAl-borate, ZnAl-borate, and MgAl-PO_4 has been studied [39]. Ye et al. prepared MgAl-CO_3 and MgAl-PO_4 LDHs and investigated their flame retardant properties in EVA [22]. With 60 wt% LDH loading, the PHRR reduction for MgAl-CO_3 and MgAl-PO_4 LDHs was 66% and 76%, respectively [22]. Nyambo et al. introduced MgAl-borate and ZnAl-borate LDHs into EVA and observed significant PHRR

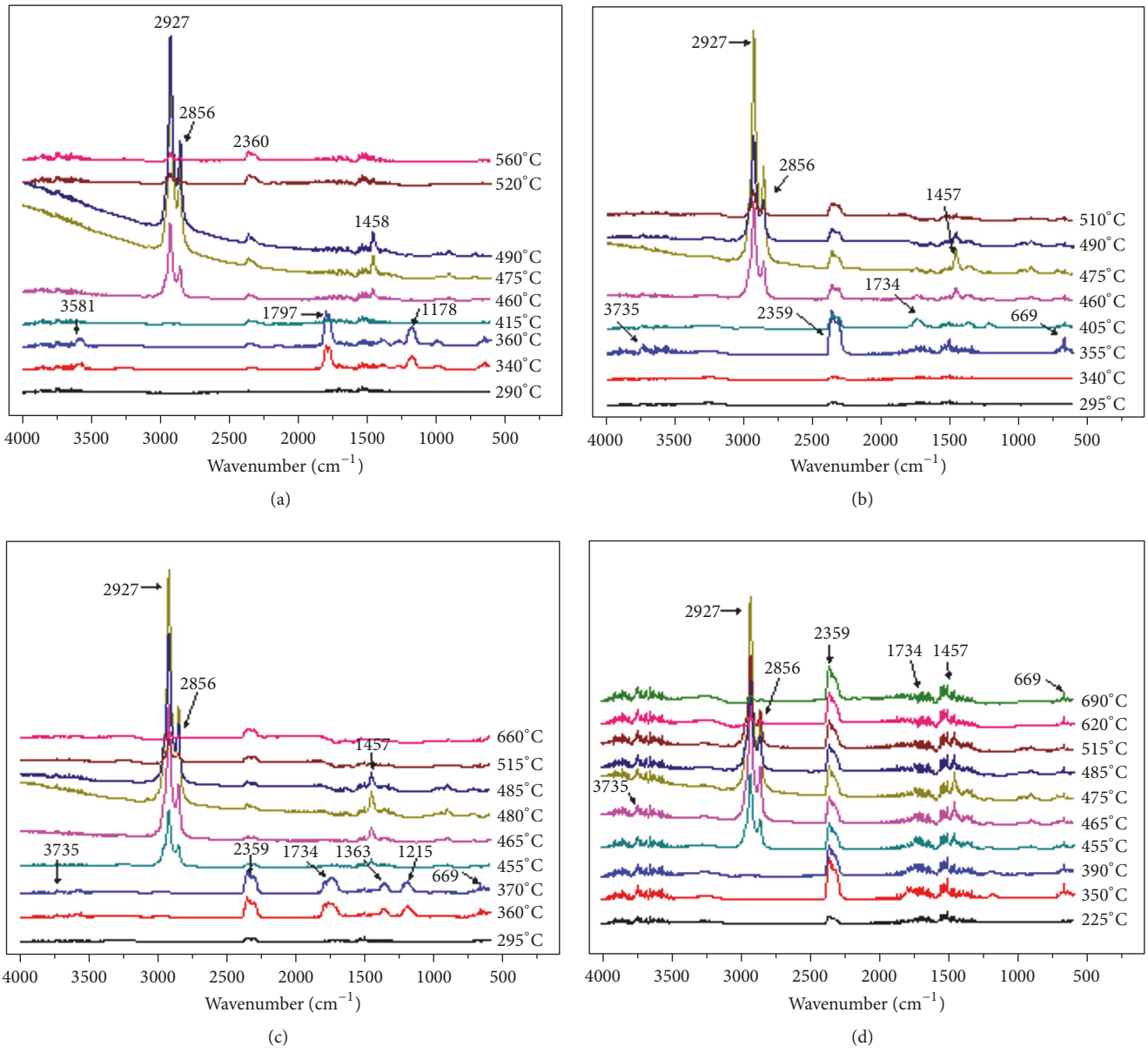

Figure 12: FTIR spectra of pyrolysis products of the composites at different temperatures: (a) EVA0, (b) EVA1, (c) EVA2, and (d)EVA3.

reductions for both LDHs. When the LDHs loading was 40 wt%, the PHRR reductions for MgAl-borate and ZnAl-borate LDHs reached 74% and 77%, respectively [40]. In this work, when the LDHs loading was 50 wt%, the PHRR reductions for MgAl-LDHs, MgFe-LDHs, and MgAlFe-LDHs were 86%, 81%, and 83%, respectively, suggesting that LDHs synthesized from bittern possesses better flame retardant performance than previously reported LDHs. Moreover, it has also been reported that when ZnMgAl-CO_3 and MgAl-CO_3 LDHs were added into EVA, the LOI values of the composites could reach 34 and 40, respectively [41]. However, the highest LOI value of the LDHs/EVA composites in this work is 29.8, which is significantly lower than previous work. So it can be concluded that LDHs synthesized from bittern are promising flame retardant additives for EVA.

4. Conclusions

This paper has proposed a new way to reuse the byproduct of seawater bittern or brine. The waste bittern contains a great amount of Mg^{2+}, which can be used to synthesize LDHs. In this study, three kinds of LDHs (MgAl-LDHs, MgFe-LDHs, and MgAlFe-LDHs) were successfully prepared from bittern using a coprecipitation method, and they were characterized by XRD and TGA. The results showed that LDHs were successfully synthesized, and the crystal structures of MgAl-LDHs were better than the other ones. Then, three kinds of LDHs were added into EVA as a halogen-free flame retardant. The results from CCT, LOI, SDT, and TG-IR showed that all the three kinds of LDHs, especially MgAl-LDHs, could greatly improve the flame retardant performance and thermal

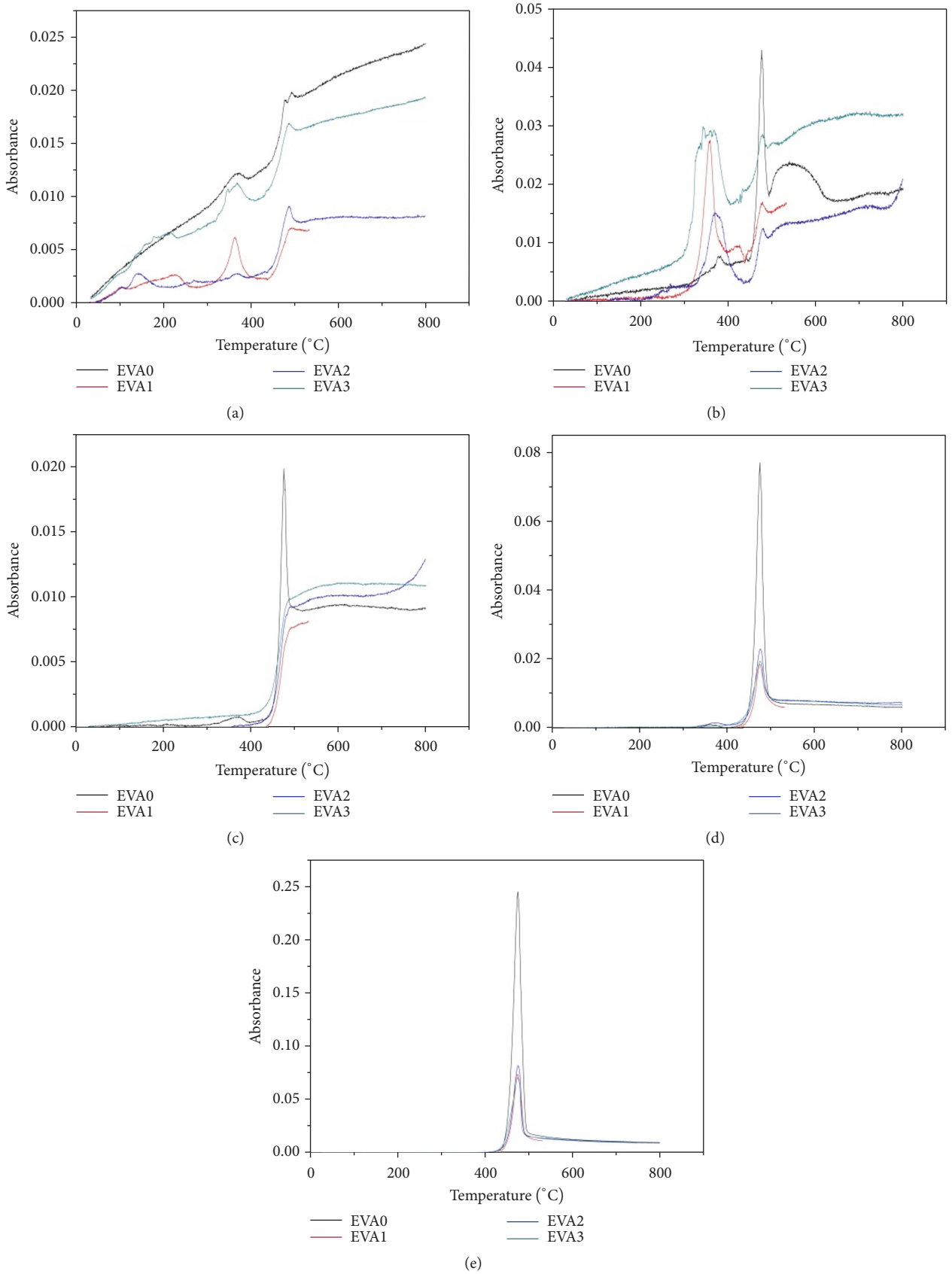

Figure 13: Variations in the evolved (a) H_2O, (b) CO_2, (c) CO, (d) carboxylic acid, and (e) aliphatic hydrocarbons gases from EVA0, EVA1, EVA2, and EVA3 samples.

stability of the composites. This is the first time that LDHs have been synthesized from bittern and then used as efficient flame retardant materials for EVA. We believe that this work will broad the way for the reuse and recovery of solid waste.

Data Availability

All data used to support the findings of this study may be released upon application to the Qingdao University of Science and Technology, who can be contacted at qdkjdx@qust.edu.cn.

Conflicts of Interest

The authors declare that there are no conflicts of interest regarding the publication of this paper.

Acknowledgments

The authors gratefully acknowledge the National Natural Science Foundation of China (no. 51572138), the Shandong Provincial Natural Science Foundation, China (ZR2018BB072), the Foundation of State Key Laboratory of High-efficiency Utilization of Coal and Green Chemical Engineering (nos. 2018-K09 and 2018-K43), and Key Laboratory of Coastal Environmental Processes and Ecological Remediation, YICCAS, Grant no. 2018KFJJ02.

References

[1] P. A. Davies and P. R. Knowles, "Seawater bitterns as a source of liquid desiccant for use in solar-cooled greenhouses," *Desalination*, vol. 196, no. 1-3, pp. 266–279, 2006.

[2] R. Liao, Y. Li, X. Yu et al., "Performance and microbial diversity of an expanded granular sludge bed reactor for high sulfate and nitrate waste brine treatment," *Journal of Environmental Sciences*, vol. 26, no. 4, pp. 717–725, 2014.

[3] M. Tedesco, E. Brauns, A. Cipollina et al., "Reverse electrodialysis with saline waters and concentrated brines: a laboratory investigation towards technology scale-up," *Journal of Membrane Science*, vol. 492, pp. 9–20, 2015.

[4] D. Han, H.-L. Cui, and Z.-R. Li, "Halopenitus salinus sp. nov., isolated from the brine of salted brown alga Laminaria," *Antonie van Leeuwenhoek-Journal of Microbiology*, vol. 106, no. 4, pp. 743–749, 2014.

[5] S. I. Lee, S. Y. Weon, C. W. Lee, and B. Koopman, "Removal of nitrogen and phosphate from wastewater by addition of bittern," *Chemosphere*, vol. 51, no. 4, pp. 265–271, 2003.

[6] A. Alamdari, M. R. Rahimpour, N. Esfandiari, and E. Nourafkan, "Kinetics of magnesium hydroxide precipitation from sea bittern," *Chemical Engineering and Processing: Process Intensification*, vol. 47, no. 2, pp. 215–221, 2008.

[7] J. Sun, Y. Dong, and C. Kong, "Manufacture of sodium-free lithium chloride from salt lake brine," *Separation and Purification Technology*, vol. 136, no. 5, pp. 309–313, 2014.

[8] L. F. Albuquerque, A. A. Salgueiro, J. L. D. S. Melo, and O. Chiavone-Filho, "Coagulation of indigo blue present in dyeing wastewater using a residual bittern," *Separation and Purification Technology*, vol. 104, no. 5, pp. 246–249, 2013.

[9] G. M. Ayoub, A. Hamzeh, and L. Semerjian, "Post treatment of tannery wastewater using lime/bittern coagulation and activated carbon adsorption," *Desalination*, vol. 273, no. 2-3, pp. 359–365, 2011.

[10] G. M. Ayoub and F. Merhebi, "Characteristics and quantities of sludge produced by coagulating wastewater with seawater bittern, lime and caustic," *Advances in Environmental Research*, vol. 6, no. 3, pp. 277–284, 2002.

[11] A. S. Sánchez, I. B. R. Nogueira, and R. A. Kalid, "Uses of the reject brine from inland desalination for fish farming, Spirulina cultivation, and irrigation of forage shrub and crops," *Desalination*, vol. 364, no. 15, pp. 96–107, 2015.

[12] J. K. Al-Handhaly, A. M. O. Mohamed, and M. Maraqa, "Impact of chemical composition of reject brine from inland desalination plants on soil and groundwater, UAE," *Desalination*, vol. 156, no. 1-3, p. 89, 2003.

[13] G. Lychnos, J. P. Fletcher, and P. A. Davies, "Properties of seawater bitterns with regard to liquid-desiccant cooling," *Desalination*, vol. 250, no. 1, pp. 172–178, 2010.

[14] H. Xu and X.-R. Deng, "Preparation and properties of superfine Mg(OH)2 flame retardant," *Transactions of Nonferrous Metals Society of China*, vol. 16, no. 2, pp. 488–492, 2006.

[15] C. Li, M. Wei, D. G. Evans, and X. Duan, "Recent advances for layered double hydroxides (LDHs) materials as catalysts applied in green aqueous media," *Catalysis Today*, vol. 247, pp. 163–169, 2015.

[16] D. Basu, A. Das, K. W. Stöckelhuber, U. Wagenknecht, and G. Heinrich, "Advances in layered double hydroxide (LDH)-based elastomer composites," *Progress in Polymer Science*, vol. 39, no. 3, pp. 594–626, 2014.

[17] J. C. A. A. Roelofs, A. J. van Dillen, and K. P. de Jong, "Base-catalyzed condensation of citral and acetone at low temperature using modified hydrotalcite catalysts," *Catalysis Today*, vol. 60, no. 3-4, pp. 297–303, 2000.

[18] K. D. Beard, D. Borrelli, A. M. Cramer, D. Blom, J. W. Van Zee, and J. R. Monnier, "Preparation and structural analysis of carbon-supported co core/pt shell electrocatalysts using electroless deposition methods," *ACS Nano*, vol. 3, no. 9, pp. 2841–2853, 2009.

[19] V. Ambrogi, G. Fardella, G. Grandolini, M. Nocchetti, and L. Perioli, "Effect of hydrotalcite-like compounds on the aqueous solubility of some poorly water-soluble drugs," *Journal of Pharmaceutical Sciences*, vol. 92, no. 7, pp. 1407–1418, 2003.

[20] A.-Y. Park, H. Kwon, A. J. Woo, and S.-J. Kim, "Layered double hydroxide surface modified with (3-aminopropyl) triethoxysilane by covalent bonding," *Advanced Materials*, vol. 17, no. 1, pp. 106–109, 2005.

[21] M. Hadnadjev-Kostic, T. Vulic, and R. Marinkovic-Neducin, "Solar light induced rhodamine B degradation assisted by TiO2-Zn-Al LDH based photocatalysts," *Advanced Powder Technology*, vol. 25, no. 5, pp. 1624–1633, 2014.

[22] L. Ye and B. Qu, "Flammability characteristics and flame retardant mechanism of phosphate-intercalated hydrotalcite in halogen-free flame retardant EVA blends," *Polymer Degradation and Stability*, vol. 93, no. 5, pp. 918–924, 2008.

[23] J. Alongi, F. Cuttica, and F. Carosio, "DNA coatings from byproducts: a panacea for the flame retardancy of EVA, PP, ABS, PET, and PA6?" *ACS Sustainable Chemistry & Engineering*, vol. 4, no. 6, pp. 3544–3551, 2016.

[24] J. Alongi, A. D. Blasio, F. Cuttica, F. Carosio, and G. Malucelli, "Bulk or surface treatments of ethylene vinyl acetate copolymers

with DNA: investigation on the flame retardant properties," *European Polymer Journal*, vol. 51, no. 1, pp. 112–119, 2014.

[25] F. Carosio, J. Alongi, C. Paravidino, and A. Frache, "Improving the flame retardant efficiency of layer by layer coatings containing deoxyribonucleic acid by post-diffusion of hydrotalcite sanoparticles," *Materials*, vol. 10, no. 7, p. 709, 2017.

[26] K. Nejati, H. Keypour, P. D. K. Nezhad, Z. Rezvani, and K. Asadpour-Zeynali, "Preparation and characterization of cetirizine intercalated layered double hydroxide and chitosan nanocomposites," *Journal of the Taiwan Institute of Chemical Engineers*, vol. 53, pp. 168–175, 2015.

[27] H. Zhang, R. Qi, D. G. Evans, and X. Duan, "Synthesis and characterization of a novel nano-scale magnetic solid base catalyst involving a layered double hydroxide supported on a ferrite core," *Journal of Solid State Chemistry*, vol. 177, no. 3, pp. 772–780, 2004.

[28] H. Zhang, K. Zou, H. Sun, and X. Duan, "A magnetic organic-inorganic composite: Synthesis and characterization of magnetic 5-aminosalicylic acid intercalated layered double hydroxides," *Journal of Solid State Chemistry*, vol. 178, no. 11, pp. 3485–3493, 2005.

[29] C. X. Jia, X. L. Chen, and Y. Qian, "Synergistic flame retardant effect of graphite powder in EVA/LDH composites," *Plastics, Rubber and Composites*, vol. 43, no. 2, pp. 46–53, 2014.

[30] M. Yoshida, P. Koilraj, X. Qiu, T. Hirajima, and K. Sasaki, "Sorption of arsenate on MgAl and MgFe layered double hydroxides derived from calcined dolomite," *Journal of Environmental Chemical Engineering (JECE)*, vol. 3, no. 3, pp. 1614–1621, 2015.

[31] L. Li, Y. Qian, and C. M. Jiao, "Synergistic flame retardant effect of melamine in ethylene-vinyl acetate/layered double hydroxides composites," *Journal of Thermal Analysis and Calorimetry*, vol. 114, no. 1, pp. 45–55, 2013.

[32] C.-X. Zhao, Y. Liu, D.-Y. Wang, D.-L. Wang, and Y.-Z. Wang, "Synergistic effect of ammonium polyphosphate and layered double hydroxide on flame retardant properties of poly(vinyl alcohol)," *Polymer Degradation and Stability*, vol. 93, no. 7, pp. 1323–1331, 2008.

[33] L. Li, Y. Qian, and C. M. Jiao, "Influence of red phosphorus on the flame-retardant properties of ethylene vinyl acetate/layered double hydroxides composites," *Iranian Polymer Journal (English Edition)*, vol. 21, no. 9, pp. 557–568, 2012.

[34] L. Shi, D. Li, S. Li, J. Wang, D. G. Evans, and X. Duan, "Structure, flame retarding and smoke suppressing properties of Zn-Mg-Al-CO3 layered double hydroxides," *Chinese Science Bulletin*, vol. 50, no. 11, pp. 1101–1104, 2005.

[35] C. Feng, Z. Li, M. Liang, J. Huang, and H. Liu, "Preparation and characterization of a novel oligomeric charring agent and its application in halogen-free flame retardant polypropylene," *Journal of Analytical and Applied Pyrolysis*, vol. 111, pp. 238–246, 2015.

[36] G. Zhang, P. Ding, M. Zhang, and B. Qu, "Synergistic effects of layered double hydroxide with hyperfine magnesium hydroxide in halogen-free flame retardant EVA/HFMH/LDH nanocomposites," *Polymer Degradation and Stability*, vol. 92, no. 9, pp. 1715–1720, 2007.

[37] Z.-B. Shao, C. Deng, Y. Tan, M.-J. Chen, L. Chen, and Y.-Z. Wang, "Flame retardation of polypropylene via a novel intumescent flame retardant: ethylenediamine-modified ammonium polyphosphate," *Polymer Degradation and Stability*, vol. 106, no. 8, pp. 88–96, 2014.

[38] J. Gong, R. Niu, N. Tian et al., "Combination of fumed silica with carbon black for simultaneously improving the thermal stability, flame retardancy and mechanical properties of polyethylene," *Polymer Journal*, vol. 55, no. 13, pp. 2998–3007, 2014.

[39] Y. Gao, J. Wu, Q. Wang, C. A. Wilkie, and D. O'Hare, "Flame retardant polymer/layered double hydroxide nanocomposites," *Journal of Materials Chemistry A*, vol. 2, no. 29, pp. 10996–11016, 2014.

[40] C. Nyambo and C. A. Wilkie, "Layered double hydroxides intercalated with borate anions: Fire and thermal properties in ethylene vinyl acetate copolymer," *Polymer Degradation and Stability*, vol. 94, no. 4, pp. 506–512, 2009.

[41] L. Shi, D. Li, S. Li, J. Wang, D. G. Evans, and X. Duan, "Structure, flame retarding and smoke suppressing properties of Zn-Mg-Al-CO3 layered double hydroxides," *Chinese Science Bulletin*, vol. 50, no. 11, pp. 1101–1104, 2005.